

RESEARCH ARTICLE

# Design and manufacturing of a single-phase induction motor: A decision aid tool approach

Yannis L. Karnavas<sup>1</sup> | Ioannis D. Chasiotis

Laboratory of Electrical Machines,  
Department of Electrical and Computer  
Engineering, Democritus University of  
Thrace, Xanthi, 671 00, Greece

## Correspondence

Yannis L. Karnavas, Laboratory of Electrical  
Machines, Department of Electrical and  
Computer Engineering, Democritus  
University of Thrace, Room 0.21, Build. B,  
Kimmeria, Xanthi, 671 00, Greece.  
Email: karnavas@ee.duth.gr

## Summary

This paper presents a simple, practical, and effective design, analysis, and selection approach of a capacitor-run single phase induction motor as a manufacturing aid tool at the early stage of the design. The standard industrial motor frame sizes as well as the current design trends of larger lengths and smaller diameters—which are not likely presented in literature—are taken into account. At first, to verify the proposed approach, a sample single phase induction motor design is obtained regarding certain requirements, based mainly on the classic output coefficient concept. Then, numerous simulations over a large number of candidate motor topologies are conducted. This series of investigations is performed initially with respect to (1) certain operational industrial criteria, (2) the number of stator and rotor slots, and (3) the rotor cage material. After the relevant results are presented and commented, a selection strategy of an appropriate design is also proposed. Also, the effect of the running capacitor value is examined. It is seen that the total design and selection procedure are verified very satisfactorily. Finally, useful conclusions from a manufacturer's point of view are also extracted, dealing with important operational characteristics of the motor, such as power factor, winding currents phase shift, total losses, starting/rated torque ratio, efficiency, and other.

## KEYWORDS

electrical machine design and manufacturing, finite element analysis, industrial motor frames, single-phase induction motor

## 1 | INTRODUCTION

While 3-phase induction motors are mainly used in commercial and industrial applications, there are cases where the use of a 3-phase power supply is not possible and subsequently single-phase induction motors (SPIM)s are adopted. The application field range of SPIMs is impressive; they are extensively used in numerous industrial, agricultural, and residential applications such as washing machines, compressors, refrigerating and kitchen appliances, heat-circulating pumps, power tools, fans, sewing machines, vacuum cleaners, grain dryers, etc. In general, there is a strong demand for SPIMs, and it can be said without exaggeration that literally millions of them are produced every year.<sup>1</sup>

The main feature of SPIMs is that if they are put into operation by means of a rotating magnetic field, then their rotor will continue to rotate even if the coils are supplied with single-phase current, which does not create a rotating magnetic field.<sup>2</sup> A SPIM that is equipped with a permanent capacitor (capacitor-run type) and that is usually designed for power outputs of 0.25 HP up to 1.5 HP presents the following characteristics and/or advantages over other types (thus, it will be the subject of study in this work): (1) it is less expensive and more reliable as it does not need any centrifugal switch, (2) it has a low starting to rated torque ratio, (3) it needs less starting current than any other design of SPIM and withstands a large load cycle, (4) it works silently while serving its load, (5) it enables adjusting its speed by changing

the voltage of the power supply, (6) it is easily reversible (can stop and change rotation direction) because of the low torque, (7) it has a relatively high efficiency and high-power factor.<sup>3</sup>

At the same time and although the design and the use of SPIMs has evolved throughout the decades, there are still some factors related to optimization and efficiency, which have remained critical to engineers. A review in the relevant technical literature shows that there are several research efforts concerning the broad aspect of SPIM performance improvement, eg, previous studies.<sup>4–10</sup> An approach to this problem through 2-level optimization is described in Jazdzynski.<sup>5</sup> A procedure to design water-cooled submersible SPIM that can be easily applicable has shown in Gundale and Kulkarni,<sup>11</sup> while a variation of stator slot design for improving the overall performance has presented in Wang et al.<sup>12</sup> Simulation results for improving the efficiency and torque of SPIMs by investigations on the impact of changing of some parameters on motor design have been also presented in Sobhani et al.<sup>13</sup> The analysis of effects of core material on the magnetic flux distribution and the performance of SPIMs has been studied in Singh and Iqbal.<sup>14</sup> Evolutionary and other “artificial intelligence” techniques like particle-swarm and ant colony optimization have also been used and their results are reported, ie, in previous studies.<sup>15–18</sup>

Design, material, and production techniques are also evolving on induction motors leading to improved efficiencies over older designs. IEEE 841 and even NEMA premium efficiency levels are now a challenge to meet and exceed. For example, new research and production techniques allow construction of SPIMs with die-cast copper rotors, allowing for even higher efficiency levels and greater longevity.<sup>19</sup>

On the basis of the above, it is revealed that there is a need not only for a simple, reliable, and cost-effective SPIM design procedure but also for a “multifeature” selection approach that can be easily followed to any application at the early stage of the design. Thus, the aim of this paper is to investigate and propose a practical, effective, and multicriteria approach as a decision aid tool, dealing with the appropriate design and selection of a certain SPIM topology among others, which meets the basic industrial standards regarding the motor's frame sizes on one hand and satisfies certain specification criteria on the other.

The proposed approach begins with a preliminary design phase described in Section 2 that is based mainly on classical motors output coefficient concept while the diameter and length of the motor are modified according to the corresponding standards frame size. In Section 3, a systematic evaluation of (1) stator/rotor slots combination and (2) the rotors bars and rings material is performed. After an appropriate design is reached, a simple but effective selection strategy is also proposed, and a parametric analysis of the required permanent capacitor to be installed is investigated also in Section 4,

to validate the appropriateness of the selected SPIM topology. Finally, Section 5 summarizes and concludes the work.

## 2 | PRIMARY DESIGN PHASE OF SPIM

In this section, the specifications of the SPIM design are set, in order for a sample design to be initiated. Following the classical design approach, the initial active length and diameter of the machine have to be determined first. In this place, the international frame size are presented and followed. The design phase starts from the specification of the motor and ends in a first geometric configuration. The overall geometric parameters are obtained analytically. Once the design is reached and validated, the remaining investigations and selection process are presented in the next section.

### 2.1 | Specifications of the SPIM under study

The design of an electric motor is performed to meet certain specifications. The most important among others are the rated power, the rated supply voltage and frequency, the rated speed, and the number of poles. Additionally, the required efficiency and power factor can also be considered as desirable characteristics. In case of a SPIM, another very important detail in the design procedure is the motor type regarding the windings configuration. Here, the permanent capacitor type is considered. Moreover, the mounting type, the performance, and insulation classes have to be taken into account. Table A1 in the Appendix shows the specifications adopted here.

### 2.2 | Frame size international standards

Dimensions of SPIMs are standardized according to the International Electrotechnical Commission -IEC-60072/1 as well as in ANSI/NEMA MG1-2010 standards.<sup>20,21</sup> In these standards, the basic dimension for the standardization of the assembly dimensions of electric machines is the height from the base to the shaft end center, designated by the letter H (Figure 1). To each height of shaft end H, a C dimension is associated, that is, a distance from the center line of mounting hole in the nearest foot to the shoulder on drive end shaft. However, to each H dimension, several B dimensions can be associated (distance between centerlines of mounting holes in feet) allowing to have either “longer” or “shorter” motors. Table 1 makes a comparison between dimensions H-A-B-C-K-D- E of IEC standard and D; 2E; 2F; BA; H; U-N-W of NEMA standard.

### 2.3 | Output equation concept considerations

The output equation of a machine plays a very important role as it is the link that connects the machine output power to

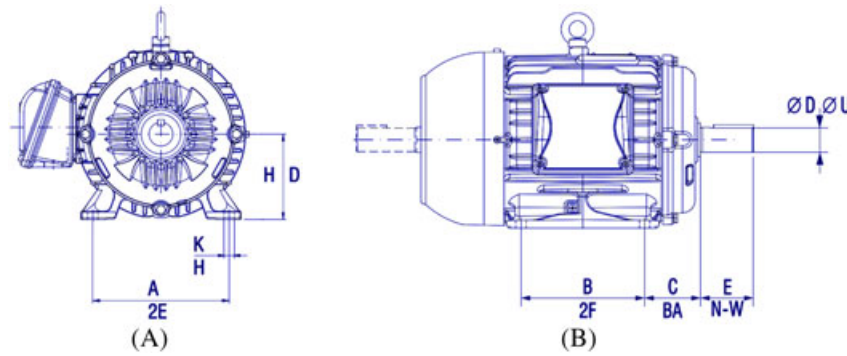


**FIGURE 1** Dimensions of “foot-mounted” single phase induction motors according to IEC/NEMA standards. (A), Front view. (B), Side view

**TABLE 1** Dimensions comparison (partial table) between IEC and NEMA standards (all dimensions in mm)

Frame Type	IEC / NEMA	H D	A 2E	B 2F	C BA	K H	D U	E N-W
63		63	100	80	40	7	11.6	23
71		72	112	90	45	7	14.6	30
80		80	125	100	50	10	19.6	40
90S/143T		90/88.9	140/139.7	100/101.6	56/57.15	10/8.7	24.6/22.2	50/57.15
90L/145T		90/88.9	140/139.7	125/127	56/57.15	10/8.7	24.6/22.2	50/57.15
100L		100	160	140	63	12	28.6	60
112S/182T		112/114.3	190/190.5	140/139.7	70/70	12/10.3	28.6/28.6	60/69.9

Abbreviation: IEC, International Electrotechnical Commission; NEMA, National Electrical Manufacturers Association.

the constructional components and electrical elements. It is essentially a mathematical formulation that associates the different physical quantities and electrical parameters and is a good base to start a design. To obtain the output equation, one has to start from the relationship that connects the input power  $P_{in}$  (W), output power  $P_{out}$  (W), and efficiency  $\eta$  of the machine, which in our case for a SPIM (number of phases  $m = 1$ ) is given by

$$P_{out} = \eta P_{in} = \eta m U_{ph} I_{ph} \cos \varphi = C_o D^2 L n_s, \quad (1)$$

where  $U_{ph}$  is a given phase voltage in (V),  $I_{ph}$  is a given phase (line) current in (A),  $\cos \varphi$  is the power factor,  $D$  is the inner stator diameter in (m),  $L$  is the active axial core length in (m), and  $n_s$  is the corresponding synchronous speed in (rpm). Also,  $C_o$  in (N/m<sup>2</sup>) is the motor's output coefficient,

$$C_o = 11 B_{av} a_c k_w \eta \cos \varphi \quad (2)$$

that involves the winding factor ( $k_w$ ), the specific electric loading ( $a_c = z_{ph} I_{ph} / (\pi D)$  in (At/m),  $z_{ph}$  is the number of conductors per phase), and the average airgap flux density ( $B_{av} = 2p \Phi_m / (\pi D L)$  in (T),  $\Phi_m$  is the magnetic airgap flux per pole in (Wb)). It should be noted here that the notation “ $2p$ ” throughout the text is referred to the number of poles ( $p$ : pole pairs). An increase on  $B_{av}$  increases the iron losses significantly but reduces the size and cost of the machine. Typical values for a 50 Hz motor lie between 0.5 and 0.9 T,

and the upper limit is set by the phenomenon of saturation of the ferromagnetic material in the stator teeth. Also, the specific electric loading is actually defined by the copper losses and limits the electric current density in the conductors for a better cooling. Again, an increase in  $a_c$  has the effect of reducing the cost and size of the motor, while at the same time, increases the copper losses, reduces the overload capacity, and leads to an increase in motors temperature. Typical values lie in the range of 5 k to 45 k At/m. The reader can refer to Pyrhoenen et al<sup>22</sup> for more details. It is apparent from Equation 1 that the quantity that is proportional to the motor's volume (referring to the inner stator diameter and the axial length of the active part of the core), ie,

$$D^2 L = P_{out} / (C_o n_s), \quad (3)$$

introduces the problem of determination of a correct combination of  $D$  and  $L$  so as to achieve the desired overall performance without exceeding mass limits, manufacturing costs and manufacturing frame limits. Therefore, the classical design approach should be altered appropriately to conform to these standards, as described next.

## 2.4 | Proposed SPIM design approach

### 2.4.1 | Stator design approach

According to classical design approach (eg, Upadhyay<sup>23</sup>), the variation of  $D_o^2 L$  as a function of horsepower for SPIMs with

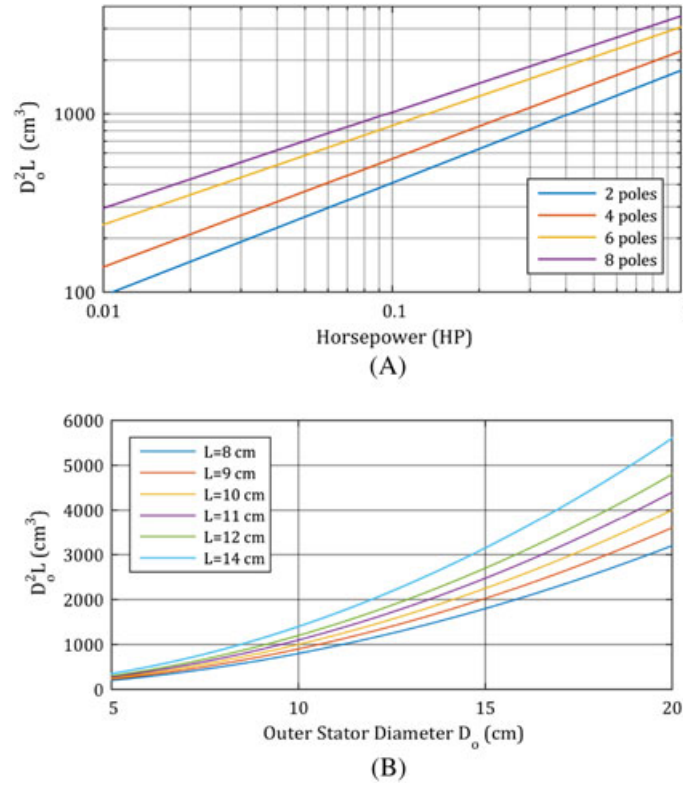


**FIGURE 2** Variation of  $D_o^2 L$  as a function of, (A), the motor's output power and, (B), the motor's outer stator diameter

2 to 8 poles has been given and is depicted in Figure 2A. Also, the relationship between  $D$  (inner) and  $D_o$  (outer) stator diameter is empirically taken the last decades in literature (within a range of 0.5 to 0.75), and a value of  $D/D_o = 0.6$  is usually used. Moreover, the length to diameter ratio for small induction machines (where the airgap is almost equal to the inner diameter of the stator) can be obtained by

$$L/D = \pi \sqrt[3]{p/(2p)}. \quad (4)$$

For our specifications of Table A1, the previous approach gives  $D_o^2 L = 2376.124 \text{ cm}^3$ ,  $L/D = 0.9895$ ,  $L = 94.25 \text{ mm}$ ,  $D = 95.25 \text{ mm}$ , and  $D_o = 158.76 \text{ mm}$ . But these starting design results are far away from international frame standards mentioned previously. Thus, the following simple procedure for them is proposed according to Figure 1 and Table 1:

- Select an appropriate frame size according to SPIM's output power.
- Consider as effective length  $L$ , the *maximum permissible length* described by the frame. This is desirable, as the current trend of manufacturers is towards larger lengths and smaller diameters, so the rotor tangential stresses can be reduced.
- By using Figure 2A, obtain  $D_o$ . For easy reference, we also introduce here Figure 2B that depicts the variation of  $D_o^2 L$  as a function of outer stator diameter ( $D_o$ ) for various lengths.

- Obtain  $D$  using the ratio  $D/D_o$ .

This approach gives the following results now: Frame size: IEC 90L (NEMA 145T), for 1.0 HP SPIM,  $L = 125 \text{ mm}$ ,  $D = 83.413 \text{ mm}$ , and  $D_o = 137.87 \text{ mm}$ . The new pole pitch can be determined now as  $\tau = \pi D/(2p)$ . The next step is the determination of the number of stator slots ( $Q_s$ ) and their geometry. Generally, there are no specific rules in literature to indicate proper selection of  $Q_s$ . However, this number is critical and affects in different ways the operation of the motor. A small  $Q_s$  contributes effectively to cost reduction, but the choice of a very small  $Q_s$  has the effect of creating very large slots with a large amount of copper in each. On the contrary, a large  $Q_s$  have the effect of reducing the leakage resistance.

This consideration reveals that it is possible for a given frame to increase the output power. Also a large  $Q_s$  reduces the problems associated with the field's harmonics and also tends to reduce the magnetic noise. However, as  $Q_s$  increases, the slot pitch ( $\tau_s = \pi D/Q_s$ ) gets smaller and smaller, and so there is a practical limit that depends on the type and the size of the motor. The number of slots per pole may usually vary up to 12. For SPIMs, it is also preferable that  $Q_s$  can be evenly divisible by the number of poles. Therefore, for our starting sample design shown here, the choice is  $Q_s = 36$ . Finally, the slot geometry used is shown in Figure 3A. This is of semiclosed trapezoidal shape and is most commonly used in contrast with the open type, as its use limits the magnetization current and reduces vibrations at teeth, and thus, a quieter

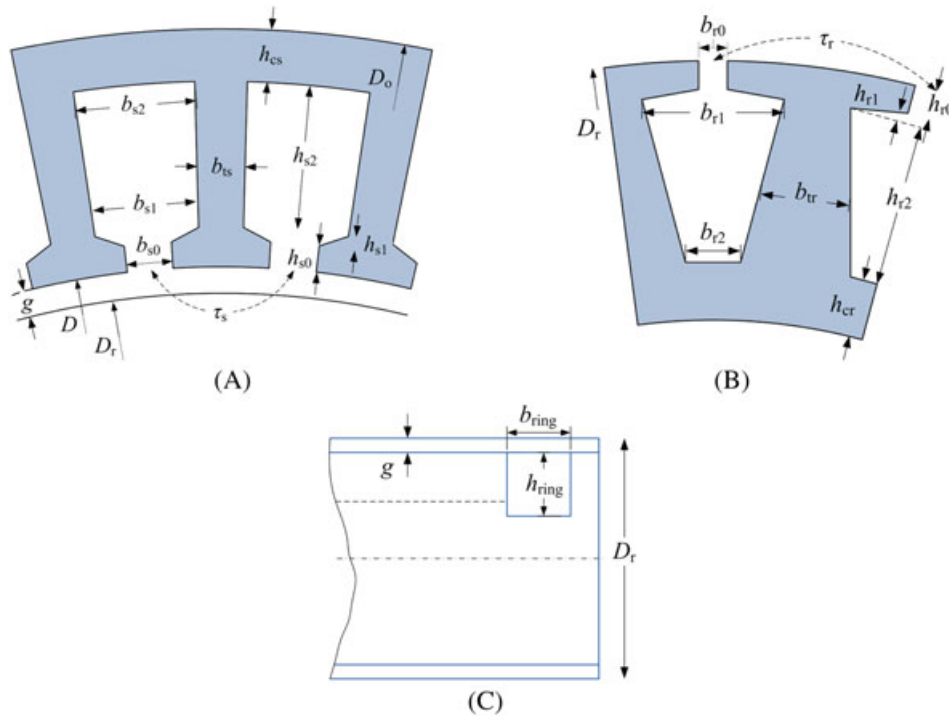


**FIGURE 3** Geometrical representations of single phase induction motor models examined, (A), stator, (B), rotor, and, (C), axial cross-section for rotor rings

operation can be achieved.<sup>19</sup> On the basis of typical commercial values for some parameters as shown in Table A2 in the Appendix, the geometry of the stator can be completed using the rest of classical design theory, eg, Upadhyay.<sup>23</sup>

## 2.4.2 | Rotor design

To proceed with the design of the rotor part, the airgap length should first be calculated. It is known that this parameter has a significant effect on the SPIM performance, and it should allow small magnetizing current drawn from the mains supply. However, the smallest possible gap technically achievable is about 0.2 mm. For small induction machines as in our case, the following relationship can be applied:

$$g = 0.007D/\sqrt{2p}. \quad (5)$$

Therefore, the outer diameter of the rotor is obtained as

$$D_r = D - 2g. \quad (6)$$

The number of rotor slots ( $Q_r$ ) is also of great importance and will be examined extensively in this study. In general, it should be chosen so as not to produce too much noise and to avoid “crawling” and “cogging” phenomena.<sup>24</sup> The set of Equations 7 describes general relations for such rotor slots selection strategy:

$$Q_r \neq Q_s$$

$$Q_r \neq \pm p, \pm 2p, \pm 5p$$

$$Q_s - Q_r \neq \pm 3p, \pm 4p, \pm 6p$$

$$Q_s - Q_r \neq \pm 1, \pm 2, \pm 4, (\pm p \pm 1), (\pm p \pm 2), (\pm 2p \pm c), c=1, 2, 3, 4. \quad (7)$$

Here, a large number (70%) of the possible combinations will be examined because we need to derive information of their influence on several performance quantities. In any case, the rotor slot pitch will be  $\tau_r = \pi D_r / Q_r$ . The rotor's slot geometry can also be varied. As it can be seen in Figure 3B, trapezoidal slot shape will be examined, as this shape has been already chosen for the stator slots. On the basis of typical commercial values for some parameters as per Table A2, the geometry of the rotor can be obtained now analytically using also the classical design theory. It should noted also that a small  $b_{r0}$  value (under 1.5 mm) shown in Table A2 has been justified in literature.<sup>25</sup> Finally, since the rotor used is of “squirrel cage” type, it is necessary to identify and size of the short-circuit rings. The size of the ring cross-section area can be calculated by

$$A_{ring} \approx A_{sr}(2 \sin(\pi p / Q_r))^{-1}, \quad (8)$$

where  $A_{sr}$  is the rotor slot area. If the radial height of the ring is  $h_{ring}$ , then the axial length is

$$b_{ring} = A_{ring} / h_{ring}. \quad (9)$$

The sectional view of the SPIMs ring geometry is shown in Figure 3C.



### 2.4.3 | Sample SPIM design results

Following the above proposed approach under the requirements, data, and constraints given, a sample SPIM was designed, having  $Q_s = 36$  and  $Q_r = 18$ . Low-carbon steel alloy (Steel-1008) was adopted for the stator and rotor cores,<sup>26</sup> while die-cast copper was selected for the rotor bars and rings. Low-carbon steel alloy is conventional structure steel used widely in industry. Carbon is added to iron because even with low-doping rate, it significantly improves the mechanical properties of this alloy. The carbon content must rather be low to maintain decent electromagnetic properties.

Figure 4 depicts various performance quantities of the redesigned SPIM (efficiency, power factor, line current, output torque, and output power) variation versus speed. It can be observed that the desired efficiency is achieved at about 1430 rpm, while the rated output power can be delivered from the motor over 1420 rpm. The starting current is about 16.25 A (giving a 4.23 ratio comparing with rated). Moreover, the starting torque is about 0.15 Nm while the rated torque obtained is 5.0 Nm at about 1467 rpm. Also, from manufacturing point of view, Figure 5 depicts the geometrical representations of the 2 equivalent—operationally—SPIM designs: before, ie, using the classical design theory approach (Figure 5A) and after, ie, using the proposed design approach (Figure 5B). The performance and geometrical characteristics of these 2 SPIMs are given in Table A3 in the Appendix. From this Table, it can be observed that all the performance quantities are improved (slightly or significantly) when the modified methodology is followed compared with the corresponding ones from the classical approach. For example, the motor's net mass (shaft and frame excluded) is equal to 13.87 kg for the first case, while for the second one, it comes to 13.14 kg. Additionally, for the same motor's volume, a higher power density is achieved. Moreover, important increment (about 55.8%) arises in the starting torque of the modified

SPIM according to the proposed procedure. Considering all the above, it is apparent that the proposed design approach can lead to very satisfactory results. Nevertheless, there are still factors that may affect the design and next section will address them, towards an analysis, improvement, and decision make strategy effort.

## 3 | SECONDARY DESIGN PHASE OF SPIM

### 3.1 | Investigation of designs on the basis of the combination of stator/rotor slots and rotor cage material

Not all of the stator/rotor slots combinations can present low-noise, no-crawling, and no-cogging phenomena (as expressed in Equation 7), thus may not be acceptable from an industrial point of view for a particular application. On the basis of this fact, a semiexhaustive search was conducted here to extract useful information and relevant conclusions. In particular, we consider that  $Q_s \in [12, 24, 36]$  and  $Q_r \in [8, 10, \dots, 34, 36]$ , and also that there are 3 candidate materials (copper, aluminum, and magnesium) for the rotor bars and rings. Therefore, a total of 135 ( $3 \times 15 \times 3$ ) SPIM models were designed separately, all of them based on the proposed design procedure described in Section 2.4.

Regarding to the materials chosen, copper and aluminum (both die cast) properties are quite well known to induction motor designers, eg, Finley and Hodowanec<sup>27</sup> and Kim et al.<sup>28</sup> The use of cast magnesium has to be justified though. Magnesium has excellent stiffness and strength-to-mass ratio compared with aluminum. It has high electrical and thermal conductivity, but less than the conductivity of copper and aluminum. It withstands high-operating temperatures and has good environmental corrosion resistance, which becomes

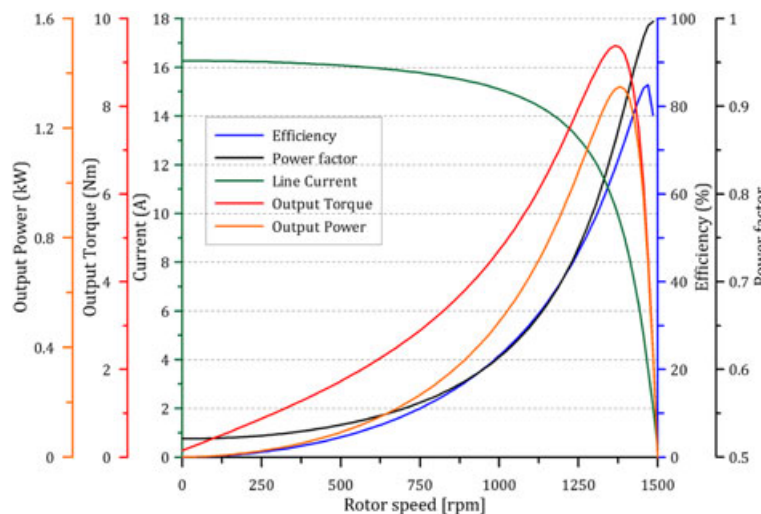


**FIGURE 4** Performance quantities of a sample designed 1 HP single phase induction motor (using the proposed approach) as a function of speed

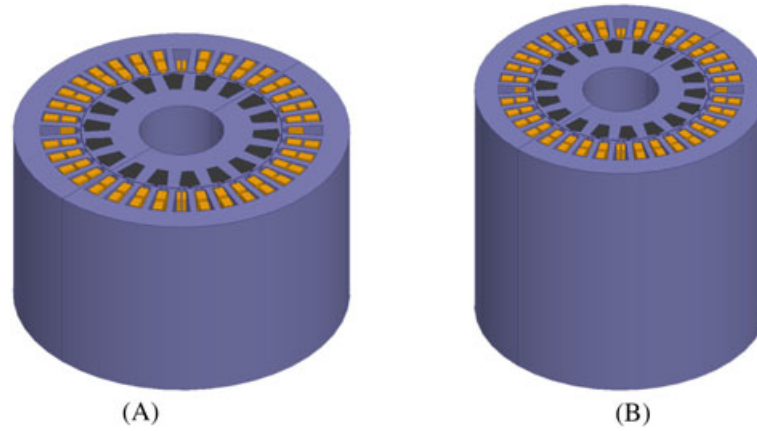


**FIGURE 5** Isometric representations (common scale) of SPIM models designed for the same operational characteristics (Table A1), (A), using classical design theory and, (B), using proposed design approach (for detailed comparison, see Table A3 w.r.t. Figure 3)

higher as new cast magnesium alloys are made. It is lighter than aluminum and copper and has a greater die life, while exhibits similar or greater mechanical properties than those of aluminum. It is used in aircrafts, wheels, actuators, power generation components, engine gearboxes, racing engine pistons, automotive and aerospace industry, and in electrical machines in the housing as well as in the squirrel cages of induction motors lately.<sup>29</sup>

The models were simulated through commercial finite element method (FEM) analysis software and quantities such as the efficiency, the power factor, the phase shift between main and auxiliary winding currents, the starting to rated torque ratio, the starting to rated current ratio, the slip, the speed, and the motor mass were recorded. Figure 6 shows the recorded results, for the 3 materials, respectively. For easiness and comparison reasons, all  $x$ -axes and  $y$ -axes are common to the subgraphs referring to the same quantity.

### 3.2 | Discussion of the results and selection considerations

By inspecting Figure 6, a common observation is that all possible topologies examined, succeeded (or so), to satisfy the design requirements and constraints set at first place. More specifically, we address and justify the main findings for each quantity:

**Efficiency.** It is illustrated that for a given number of stator slots  $Q_s$ , the larger the number of rotor bars  $Q_r$ , the greater the motor's efficiency. However, the efficiency seems to be stabilized at a value around  $Q_r=16$ . Through postprocessing analysis of the derived results, an additional study was performed through FEM (not shown here) regarding the variation of different type of losses (loss decoupling), where the following were observed:

- Copper losses in the main and auxiliary winding are higher for topologies with  $Q_r < 16$ , because of the

higher absorbed motor's line current. After this specific number of rotor bars and for any of the 3 applied materials, this type of losses exhibit low variation.

- Rotor bars ohmic losses exhibit the same behavior.
- Core and frictional losses tend to be the same as the number of rotor slots  $Q_r$  increases.
- For a small  $Q_r$ , the capacitor losses becomes high as the capacitor voltage increases. Then as  $Q_r$  increases and around  $Q_r=16$ , the value of capacitor losses is stabilized around a value and may show little variation in some cases.

A higher efficiency variation is observed at topologies with magnesium for rotor bars or with number of stator slots  $Q_s=12$ .

Also, as per the 3 materials used, the topologies with  $Q_s = 24$  exhibit the highest efficiency, followed by those with  $Q_s = 36$  and finally those with  $Q_s = 12$ . Actually, the efficiency variation observed between  $Q_s = 24$  and  $Q_s = 36$  is less than 1% in the case of copper, less than 0.6% in the case of aluminum, and less than 0.5% in the case of magnesium. The better performance presented by the topologies with  $Q_s = 24$  is due to the fact that these structures while having greater average rotor losses w.r.t. the corresponding ones with  $Q_s = 36$ , exhibit considerably lower average stator losses. Also, structures with  $Q_s = 12$  are less efficient, especially for a small number  $Q_r$ , while in case of magnesium, they hardly meet the standards set. Regarding the materials, copper is the one that gives the highest efficiency, followed by aluminum and finally magnesium. The high-electrical conductivity of copper compared with the other 2 (the magnesium conductivity is almost 63% lower than that of copper while the aluminum conductivity is about 51% lower), increases significantly the motor's performance. It was also calculated, that the average losses in the rotor in the case of copper is about 36% of the losses occur in the rotor with magnesium, and 48% compared with those of aluminum rotor.

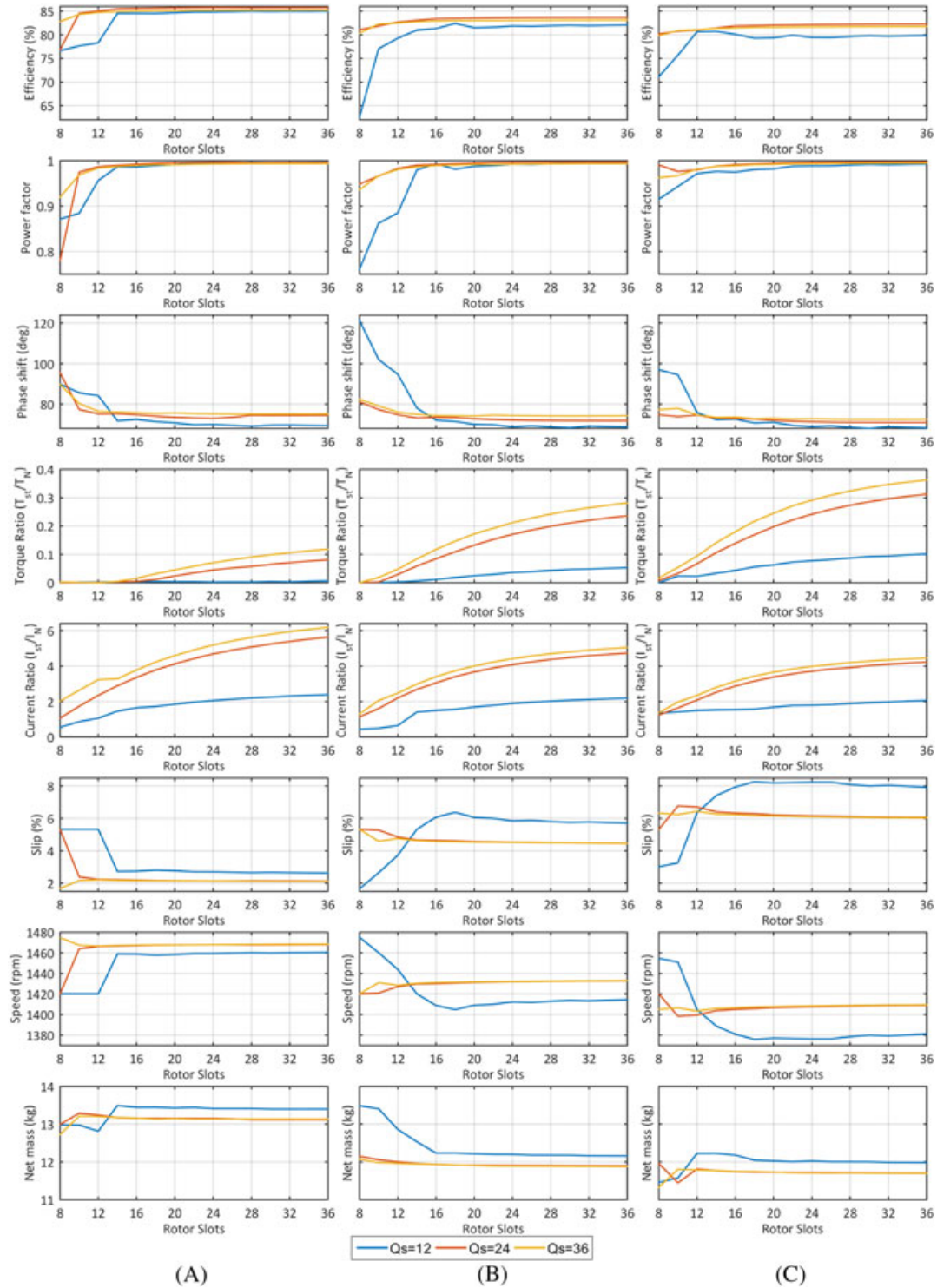


**FIGURE 6** Performance of 135 SPIM models designed, using (A), copper, (B), aluminum and (C), magnesium for rotor bars and rings (common axes to all same quantities)

On the basis of the above, it can be seen that SPIM's efficiency levels may exceed the typical values (55%-76%), which are usually met in literature or are shown in manufacturers commercial catalogues. However, the modified proposed methodology is complied with *DOE Energy Conservation Standards for small electric motors*, in

which SPIMs of rated output power within a range 0.25 to 3.0 HP were also included.<sup>30</sup> This standard is valid since March 2015 and determines that the minimum expected efficiency for a 1 HP SPIM (with rotor bars made by die-cast copper) is equal to 82.6%. That is why, a minimum efficiency value equal to 80% was selected here as a design



constraint for all the derived topologies with 3 different materials for rotor bars. Moreover, IEEE 841 standards and NEMA design instructions for high-efficiency motors, such as smaller air gap size, usage of larger wire gauge for stator windings, and incorporation of larger motor effective length, were also taken into account.

**Power factor.** During the design phase, a high-power factor goal was set, compared with values typically found in (or requested by) the industrial needs. Despite that, the results of the proposed designs show that this goal has been achieved, since all topologies combinations ( $Q_s/Q_r$ ) with few exceptions (12/8, 12/10, and 24/8 for copper and 12/8, 12/10, and 12/12 for aluminum) present a value greater than 0.9 and almost equal to unity. Even though all differences may be negligible, it can be observed that for any material, topologies with  $Q_s = 12$  present lower power factor values relative to the  $Q_s = 24$  or  $Q_s = 36$  ones, while those with  $Q_s = 24$  exhibit slightly larger values than those of  $Q_s = 36$ . Also, the greater the  $Q_r$ , the greater the power factor.

**Phase shift between winding currents.** It is shown that a small  $Q_r$ , the angle between the currents of the main and auxiliary windings  $\theta$ , becomes high ( $> 90^\circ$ ). Then, as  $Q_r$  increases, there is a declining trend. Beyond a certain  $Q_r$ ,  $\theta$  is “stabilized” around a value and may show little variation in some cases (as in the case of  $Q_s = 12$ ). With respect to an angle of  $90^\circ$ —which is considered as ideal—a lower value of  $\theta$  is preferable rather than higher one, because the latter case will result in torque fluctuations, higher ripple, and vibrations that are not easily absorbed by the shaft, resulting in noisy operation.<sup>31</sup> Regarding to the materials used, it seems that there is an advantage of copper, in which  $\theta$  reaches  $69^\circ$ ,  $74^\circ$ , and  $75^\circ$  for  $Q_s = 12$ , 24, and 36, respectively, and is greater than the corresponding ones of other 2 materials ( $68^\circ$ ,  $71^\circ$ , and  $74^\circ$  for aluminum and  $68^\circ$ ,  $70^\circ$ , and  $72^\circ$  for magnesium). However, an investigation as per the value of capacitor that will follow in the next section will show the influence of the capacitor on  $\theta$ .

**Starting to rated torque ratio.** All examined models succeeded to achieve a torque equal to 5 Nm. Moreover, considering the results for the  $T_{st}/T_N$  ratio results, the following are observed:

- All topologies (except 36/34 and 36/36 for magnesium) achieve a ratio of less or equal to 0.35.
- The starting torque becomes greater as  $Q_r$  increases. Therefore, the maximum starting torque is achieved for  $Q_r = 36$ .
- For any material applicable, topologies with  $Q_s = 36$  present higher  $T_{st}$  values compared with those with  $Q_s = 12$  and 24. Therefore, the case with  $Q_s = 12$  can be selected only if it will be combined with a large  $Q_r$  in applications where the starting torque is not a key priority.

- In terms of materials, it is observed that magnesium exhibits the higher starting torque compared with copper or aluminum. Indicatively, the 12/36 (lowest  $Q_s$ ) magnesium combination develops 0.52 Nm of starting torque, where the 36/36 (highest  $Q_s$ ) copper one exhibits only 0.57 Nm. The previous finding can be explained explicitly, if we consider the materials' conductivities. A material with higher conductivity (copper) presents a lower rotor resistance, so during starting (or high-slip values), the depended developed torque is also low. Indeed, the average rotor resistance of the models examined was found  $2.5\Omega$ ,  $5\Omega$ , and  $6.5\Omega$  for copper, aluminum, and magnesium respectively.
- The opposite applies for maximum (break-down) torque, which its behavior is varying in an inversely proportional way to the total (stator and rotor) resistance and inductance. Thus, we found here 12.53, 11.15, and 10.43 Nm for copper, aluminum, and magnesium, respectively (for the 36/36 models).

**Starting to rated current ratio.** For this constraint, the following observations arose:

- For every material used, topologies with  $Q_s = 12$  present the lower  $I_{st}/I_N$  values. The opposite occurs for  $Q_s = 36$ , with cases of  $Q_s = 24$  lying somewhere between.
- The larger the  $Q_r$ , the larger the  $I_{st}/I_N$ . Therefore, the higher values are met in 36/36 topologies.
- Comparing aluminum and magnesium with copper, the latter presents the higher values to the corresponding ones of the first 2 materials.
- Copper presents slightly less rated current, while exhibits larger starting currents because of its high conductivity and hence low resistance. This may be judged as an undesirable characteristic in some applications. In average percent terms, comparing copper for topologies with  $Q_s = 12$ , 24, and 36, there is a 7%, 15%, and 17.7% higher starting current compared with aluminum and 8.2%, 16%, and 21% compared with magnesium, to all corresponding topologies.
- Consequently, concerning the relevant constraint set (Table A1), one can choose from the following options: (1) Copper:  $Q_r \leq 36$  for  $Q_s = 12$ ,  $Q_r \leq 22$  for  $Q_s = 24$ , and  $Q_r \leq 18$  for  $Q_s = 36$ , (2) Aluminum:  $Q_r \leq 36$  for  $Q_s = 12$ ,  $Q_r \leq 30$  for  $Q_s = 24$ , and  $Q_r \leq 24$  for  $Q_s = 36$ , (3) Magnesium:  $Q_r \leq 36$  for  $Q_s = 12$ ,  $Q_r \leq 36$  for  $Q_s = 24$ , and  $Q_r \leq 32$  for  $Q_s = 36$ .

**Motor mass.** Cases with  $Q_s = 12$  exhibit a heavier machine by 300 to 400 gr than those of  $Q_s = 24$  and

$Q_s = 36$ , respectively. In general, for a given  $Q_s$ , as  $Q_r$  increases and after a certain value, the mass is stabilized. It can be said that the deviations observed for low  $Q_r$  is due to the different requirements that are “fulfilled” by a specific topology as per, ie, the number of turns and conductor’s cross section, to achieve the desired rated data.

Regarding to materials, the average mass for all topologies is 13.23, 12.01, and 11.82 kg for copper, aluminum, and magnesium, respectively. These differences lie mainly in the rotor cage mass that is found to be 1.78, 0.54, and 0.36 kg for the 3 materials (they present very different mass densities). The greater cage mass in the case of copper, combined with the higher price per kilogram (\$/kg) of material, increases the manufacturing cost of the cage and therefore the total cost. Finally, the heavier cage increases the inertia of the rotor. This may improve the motor operation, but can be a disadvantage in certain applications in which, for example, the motors often change direction of rotation at high speeds.

#### 4 | DECISION STRATEGY AND RUN CAPACITOR PARAMETRIC INVESTIGATION

It is evident up to now that the proper selection of single SPIM topology is not a matter of a standard procedure. Instead, a thorough insight of application-specific design requirements, industrial practice/standards, and parametric analyses may lead to a final decision. For our study, we propose and adopted the following simple but effective strategy:

**Step 1:** Some models that do not comply to “crawling,” “cogging,” and noise requirements should be rejected in the first place. In this study, we choose the more strict scenario, so all models (of the 135) that did not satisfy Equation 7 were discarded. It should be noted here that this strict policy may result in the exclusion of some common

stator/rotor slot combinations (eg,  $Q_s = 36$  and  $Q_r = 28$ ) currently used in industry).

**Step 2:** From the models remained, all models that did not satisfy completely the requirements of Table A1 were also discarded. In this way, 15 candidate models remained (5 from each material applied) and are shown in Tables 2 to 4 along with 6 quantities of interest.

**Step 3:** The total universe of discourse of each quantity was evenly divided into 5 regions, namely, VH = *veryhigh*, H = *high*, M = *medium*, L = *low*, and VL = *verylow*.

**Step 4:** A ranking is then performed according to the “score” of each candidate model, by counting the times by which a certain quantity region was achieved. The results were summarized in Tables 2 to 4 (every second row). It can be seen that only 5 models are prevail, 4 of them with magnesium for rotor cage, and 1 with copper.

**Step 5:** If there is more than 1 “winner” (like in our case), someone can take into consideration the results of Section 3.1 and the relevant discussion of Section 3.2. Following this strategy and for the scope of this study, the topology with  $Q_s = 36$  and  $Q_r = 26$  was finally selected, since it presented the highest torque ratio and the highest efficiency. A final investigation was performed regarding the value of the run-capacitor ( $C_{run}$ ). It should be mentioned here that all previous 135 models have been simulated with a capacitance calculated through<sup>24</sup> (classical design theory) which was 18  $\mu$ F. Since the effects of  $C_{run}$  are of great importance,<sup>32</sup> a parametric analysis was conducted in the range of 10  $\mu$ F – 40  $\mu$ F (with a step of 0.2  $\mu$ F) applied to the final selected SPIM topology. Once the correct  $C_{run}$  value is determined, the industry standards like IEC-60252-1 or EIA-456-A that apply to metalized film capacitors for AC applications should be followed then by the manufacturer. The results of the parametric investigation are shown in Figure 7. The following comments may apply:

**TABLE 2** Candidate single-phase induction motor models performance and ranking. Rotor conductors material: *Copper*

$Q_s$	$Q_r$	$\eta$ , %	$\cos\phi$	$\theta$ , deg	$T_{st}/T_N$	$I_{st}/I_N$	$M$ , kg	Rank
36	18	85.0685	0.991214	75.4272	0.031522	4.235890	13.1346	
		<b>VH</b>	<b>VH</b>	H	VL	VL	VL	2
36	14	84.905	0.987419	76.1198	0.004301	3.285584	13.1755	
		<b>VH</b>	H	<b>VH</b>	VL	L	VL	2
24	14	85.4631	0.989727	75.3314	0.003014	2.896599	13.1716	
		<b>VH</b>	H	H	VL	M	VL	1
24	10	84.5344	0.974828	77.3586	0.000950	1.735979	13.2863	
		<b>VH</b>	L	<b>VH</b>	VL	<b>VH</b>	VL	3
12	36	84.9797	0.996529	69.3703	0.006623	2.393689	13.3984	
		<b>VH</b>	<b>VH</b>	VL	VL	H	VL	2

Abbreviations: H, high; L=low, M, medium; VH, very high; VL, very low.

**TABLE 3** Candidate single-phase induction motor models performance and ranking. Rotor conductors material: *Aluminum*

$Q_s$	$Q_r$	$\eta, \%$	$\cos\varphi$	$\theta, \text{deg}$	$T_{st}/T_N$	$I_{st}/I_N$	$M, \text{kg}$	Rank
36	22	83.0174	0.991569	74.5659	0.192240	4.236532	11.8925	
		M	VH	H	H	VL	VH	2
36	20	83.0119	0.991672	74.0981	0.172320	4.013581	11.9065	
		M	VH	H	M	VL	VH	2
24	14	83.0474	0.990088	73.1171	0.059101	2.690646	11.9585	
		M	H	M	VL	M	VH	1
24	10	81.8613	0.966305	77.3330	0.002264	1.611883	12.0567	
		L	VL	VH	VL	VH	H	2
12	36	82.0488	0.99462	68.7002	0.053370	2.194302	12.1581	
		L	VH	VL	VL	H	H	1

Abbreviations: H, high; L=low, M, medium; VH, very high; VL, very low.

**TABLE 4** Candidate single-phase induction motor models performance and ranking. Rotor conductors material: *Magnesium*

$Q_s$	$Q_r$	$\eta, \%$	$\cos\varphi$	$\theta, \text{deg}$	$T_{st}/T_N$	$I_{st}/I_N$	$M, \text{kg}$	Rank
36	26	81.6979	0.993847	72.6137	0.308881	4.105029	11.7060	
		L	VH	M	VH	VL	VH	3
36	22	81.6511	0.993041	72.7024	0.271250	3.843508	11.7128	
		L	VH	M	VH	VL	VH	3
24	34	82.2654	0.997257	70.9154	0.304826	4.174180	11.7092	
		M	VH	L	VH	VL	VH	3
24	14	81.4449	0.987951	73.0405	0.106349	2.528336	11.7697	
		L	H	M	L	H	VH	1
12	36	79.8592	0.992728	68.2676	0.101484	2.059337	11.9818	
		VL	VH	VL	L	VH	VH	3

Abbreviations: H, high; L=low, M, medium; VH, very high; VL, very low.

- **Efficiency:** The maximum value obtained was 82.16% for a 23.8  $\mu\text{F}$  capacitor (w.r.t. 81.89% for 18  $\mu\text{F}$ ). Also, efficiency decreases beyond 24  $\mu\text{F}$ .
- **Power factor:** A unity power factor is obtained for 24  $\mu\text{F}$  (this quantity found 0.993 for 18  $\mu\text{F}$ ), and this specific value is observed until 26  $\mu\text{F}$ . Beyond 26  $\mu\text{F}$ , the power factor decreases. This can be justified according to Equation 1 where for a given output power and voltage, the power factor should vary inversely with the current. Nevertheless, this variation range is relatively small (0.96–1.0).
- **Phase shift:** As expected, the angle  $\theta$  is increasing as the capacitance increases. The “ideal” 90° can be obtained by using a 31  $\mu\text{F}$  capacitor. However, 24  $\mu\text{F}$  ensures an almost 82° phase shift, which is satisfactory enough, compared with 72.61° given initially by 18  $\mu\text{F}$ .
- **Current:** The rated current is decreasing as the capacitance increases. The minimum value obtained was 3.94. Beyond 24  $\mu\text{F}$ , the current presents upward trend, exhibiting opposite behaviour comparing with the power factor.
- **Current ratio:** This ratio follows an upward behaviour giving a maximum value of 4.12 where the capacitance is 19.6  $\mu\text{F}$ , while beyond this value starts to decrease continuously. Here, there is an insignificant (4.105 – 4.096 = 0.009) difference when either 18  $\mu\text{F}$  or 24  $\mu\text{F}$  is used.
- **Torque ratio:** It is verified that the larger the capacitor, the larger the starting torque, which combined with the constant rated torque value leads to a increasing torque ratio.
- **Slip:** The slip variation through the capacitance range examined is very small (6.36%–5.88%). A choice of  $C_{\text{run}}=24 \mu\text{F}$  provides a 6.0% slip with a corresponding rotor speed of 1410 rpm.
- **Current density:** To ensure that the designed and selected SPIM is able to operate under free-cooling conditions (this was not set as a constraint initially, but is a desirable feature in this type of motors anyway), the current densities of both the main and auxiliary windings were examined. According to industrial standards, current density should be in the range of 3.1 to 6.2 A/mm<sup>2</sup> for enclosed type motors, while it can be 9.3 to 12.4 A/mm<sup>2</sup>

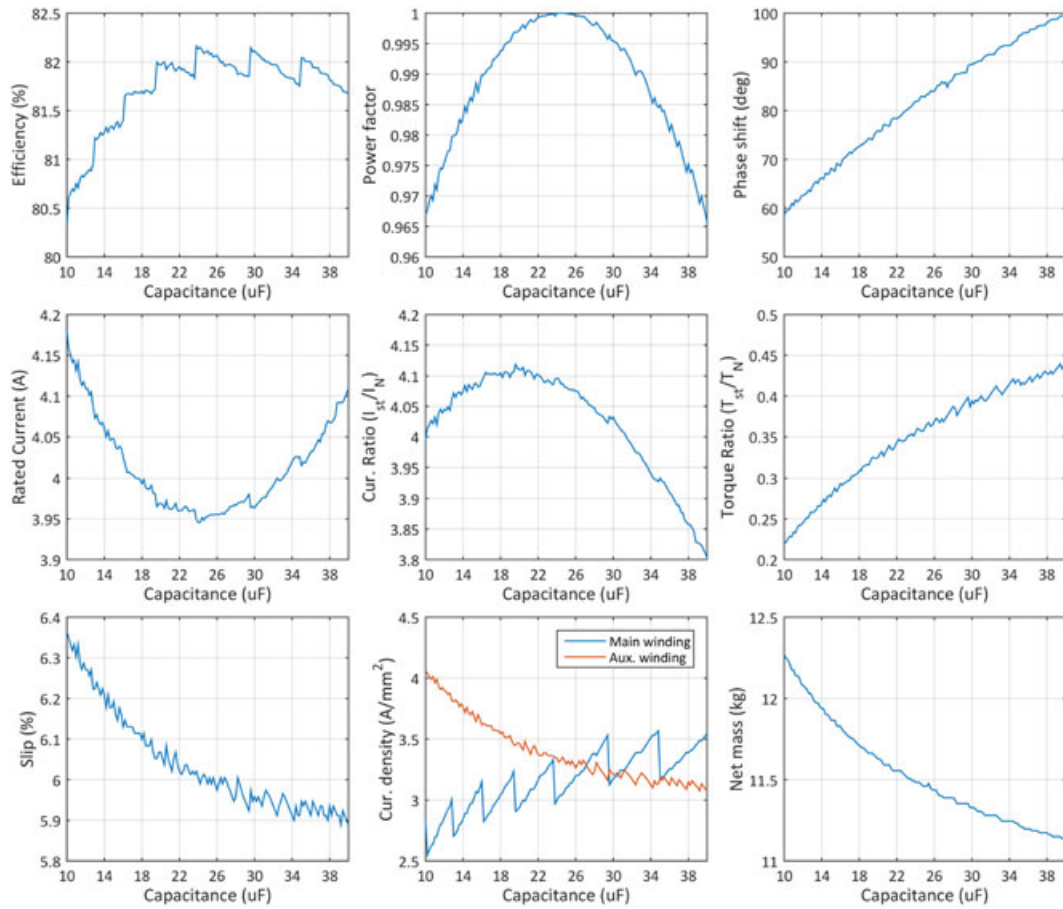


**FIGURE 7** Performance of finally selected SPIM topology ( $Q_s=36$ ,  $Q_r=26$ , and magnesium for rotor cage), with respect to run capacitor variation

for air-vented or open frame constructions. From Figure 7, it is clear that the worst case for the main winding is  $4.06 \text{ A/mm}^2$  at  $10 \mu\text{F}$ , while the corresponding one for the auxiliary winding is  $3.57 \text{ A/mm}^2$  at  $34.8 \mu\text{F}$ . That means that the selected and designed SPIM can be manufactured even using a totally enclosed frame. For reference, the windings current densities for  $24 \mu\text{F}$  capacitor are  $3.34 \text{ A/mm}^2$  and  $2.99 \text{ A/mm}^2$ , respectively.

- **Mass:** An exponentially decreasing behaviour is observed. This can be explained if we consider that the number of turns of the auxiliary winding was modified as the capacitance was increased, while the number of turns in the main winding remained constant. As a result, less copper was gradually used, and consequently, the overall mass was reduced. For a  $24 \mu\text{F}$  capacitor, SPIM's mass is  $11.48 \text{ kg}$ , where, for reference, it was found  $11.70 \text{ kg}$  for  $18 \mu\text{F}$ .

For completeness purposes, it is finally mentioned that the selection strategy of the main and auxiliary windings, commonly used in industrial available SPIMs (based on classical design theory), is also verified by the proposed design approach. The number of turns used for the auxiliary winding ( $N_a$ ) was always found greater than the corresponding one of

the main winding ( $N_m$ ). The ratio  $a = N_a/N_m$  range is 1.00 to 1.30 in all the developed models. Also, this range corresponds to a 0.7 to 0.8 range of the main winding current ( $I_m$ ) to line current ( $I_{ph}$ ) ratio, which is desirable according to Boldea and Nasar.<sup>24</sup> The abovementioned characteristics are illustrated in Table A4 in the Appendix, along with the main and auxiliary winding resistances ( $R_m$ ,  $R_a$ ), and the main and auxiliary winding reactances ( $X_m$ ,  $X_a$ ) of the candidate SPIM models (presented in Tables 2-4).

After all the above considerations, a  $C_{\text{run}}$  value of  $24 \mu\text{F}$  is finally chosen.

## 5 | CONCLUSIONS

The paper presented a design and analysis approach for single-phase induction motors mainly from a manufacturing perspective. Standard industrial frame sizes were taken into account, and also, some strict constraints were set to meet higher efficiency applications. Several combinations for stator/rotor slots were investigated, and different materials for rotor bars and rings were examined: die-cast copper (as the most commonly used material), die-cast silicon aluminum (as another important material for SPIMs), and die-cast magnesium (as an alternative and potential choice). Through a large



number of models that were designed and simulated, their relevant results were presented and commented thoroughly. Furthermore, the effect of the running capacitor was shown via a parametric investigation, and a simple selection strategy was proposed as a decision aid tool for the proper selection and manufacturing of an application specific suitable motor.

## REFERENCES

- Alger PL, Arnold RE. The history of induction motors in America. *Proc IEEE*. 2005;64(9):1380–1383.
- Sawhney AK. *A Course in Electrical Machine Design*. 4th ed. Delhi, India: Dhanpat Rai & Sons; 1977.
- Say MG. *Electrical Alternating Current Machines*. 5th ed. London, UK: Longman Scientific & Technical; 1983.
- Huang H, Fuchs EF, White JC. Optimization of single-phase induction motor design Part II: the maximum efficiency and minimum cost of an optimal design. *IEEE Trans Energy Convers*. 1988;3(2):357–366.
- Jazdzynski W. Multicriterial optimization of squirrel-cage induction motor design. *IET Electr Pow Appl (IEE Proc B)*. 1989;136(6):299–307.
- Fuchs EF, Vandenput AJ, Holl J, White JC. Design analysis of capacitor-start, capacitor-run single-phase induction motors. *IEEE Trans Energy Convers*. 1990;5(2):327–336.
- Kirtley JL, Cowie JG, Brush EF, Peters DT, Kimmich R. Improving induction motor efficiency with diecast copper rotor cages. *IEEE PES General Meeting*, Tampa, Florida, USA; 2007:1–6.
- Mera R, Campeanu R. Optimal performance of capacitor run single phase induction motor. *IEEE Proc. of 13th Intl. Conf. on Optimization of Electrical and Electronic Equipment (OPTIM)*, Brasov, Romania; 2012:718–723.
- Faiz J, Sharifian MBB. Comparison of two optimization techniques for the design of a three-phase induction motor using three different objective functions. *Euro Trans Electr Pow*. 1995;5(3):199–205.
- Tootoonchian F, Nasiri-Gheidari Z, and Lesani H. Design, analysis, and implementation of extra low air-gap single-phase axial-flux induction motors for low-cost applications. *Int Trans Electr Energ Syst*. 2016;26(12):2516–2531.
- Gundale VA, Kulkarni MS. A practical approach to the design & implementation of a water cooled single phase submersible motor. *Int J of Eng Res & Appl*. 2012;2(1):299–304.
- Wang S, Kang J, Noh J. Topology optimization of a single-phase induction motor for rotary compressor. *IEEE Trans Magn*. 2004;40(3):1591–1596.
- Sobhani S, Yaghobi H, Samakoosh M. Optimized efficiency & torque in the single-phase induction motor by adjusting the design parameters. *IEEE Proc. of 12th Intl. Conf. on Env. and Electr. Eng. (EEEIC)*, Wroclaw, Poland; 2013:237–241.
- Singh G, Iqbal MA. Computational design and analysis of core material of single-phase capacitor run induction motor. *Int J Eng Res & Appl*. 2014;4(7):20–25.
- Kim MK, Lee CG, Jung HK. Multiobjective optimal design of three-phase induction motor using improved evolution strategy. *IEEE Trans Magn*. 1998;34(5):2980–2983.
- Subramanian S, Bhuvaneshwari R. Optimal design of single-phase induction motor using particle swarm optimization. *COMPEL the Intl J Comp Math Electr Electron Eng*. 2007;26(2):418–430.
- Sakthivel VP, Bhuvaneshwari R, Subramanian S. Economic design of three-phase induction motor by particle swarm optimization. *J Electromagn Anal & Appl*. 2010;2:301–310.
- Prakash PS, Aravindhababu P. Multiobjective design of induction motor using ant colony optimization. *ARPJ Eng Appl Sci*. 2015;10(10):4449–4455.
- Malinowski J, McCormick J, Dunn K. Advances in construction techniques of AC induction motors: preparation for super-premium efficiency levels. *IEEE Trans Ind Appl*. 2004;40(6):1665–1670.
- IEC 60072-1 Intl. Standard: Dimensions and output series for rotating electrical machines—part 1: frame numbers 56 to 400 and flange numbers 55 to 1080, clauses 2, 3, 4.1, 6.1, 7 and 10, and Tables 1, 2 and 4, pertain to “IEC metric equivalents” dimensions. *International Electrotechnical Commission*, Geneva, Switzerland; 1991.
- ANSI/NEMA MG 1-2011 Standard: American national standard motors and generators: National Electrical Manufacturers Association, approved by American National Standards Institute, Inc; 2011.
- Pyrhonen J, Jokinen T, Hrabovcova V. *Design of Rotating Electrical Machines*. West Sussex, UK: John Wiley & Sons Ltd.; 2008.
- Upadhyay KG. *Design of Electrical Machines*. New Delhi: New Age International Ltd. Publishers; 2011.
- Boldea I, Nasar SA. *The Induction Machines Design Handbook*, 2. Boca Raton, FL: Taylor & Francis Group, CRC Press; 2010.
- Jang GH, Park SJ. Characterization of a single-phase induction motor due to the effect of slot opening. *IEEE Trans Magn*. 2004;40(4):2065–2067.
- Aho T, Sihvo V, Merg J, Pyrhonen J. Rotor materials for medium-speed solid-rotor induction motors. *IEEE Intl. Conf of Electric Machines & Drives (IEMDC)*, Antalya, Turkey; 2007:525–530.
- Finley WR, Hodowanec M. Selection of copper versus aluminum rotors for induction motors. *IEEE Trans Ind Appl*. 2001;37(6):1563–1573.
- Kim K, Lim SB, Lee J. Design of rotor slot of single phase induction motor with copper die-cast rotor cage for high efficiency. *IEEE Proc. of 31st Intl. Conf. on Telecom. Energy (INTELEC)*, Incheon, South Korea; 2009:1–4.
- Luo AA. Magnesium casting technology for structural applications. *J Magnesium Alloys*. 2013;1(1):2–22.
- Washington State University Energy Program. Premium Efficiency Motor Selection and Application Guide: A Handbook for Industry. prepared for the U.S. Department of Energy Efficiency and Renewable Energy, Advanced Manufacturing Office, DOE/GO-102014-4107; February 2014.
- Beran L, Mejdr F. Single-phase induction motor noise caused by improper manufacturer design. *IEEE Proc. of Intl. Workshop of Electronics, Control, Measurement, Signals and their Application to Mechatronics (ECMSM)*, Liberec, Czech; 2015:1–6.
- Muljadi E, Zhao Y, Liu TH, Lipo TA. Adjustable AC capacitor for a single-phase induction motor. *IEEE Trans Ind Appl*. 1993;29(3):479–485.

**How to cite this article:** Karnavas YL, Chasiotis ID. Design and manufacturing of a single-phase induction motor: A decision aid tool approach. *Euro Trans Electr Power*. 2017;e2357. <https://doi.org/10.1002/etep.2357>

## APPENDIX

## Problem Parameters

**TABLE A1** Single-phase induction motor under study design specifications

Quantity	Value/Type
Rated power, $P_N$	750 W (1 HP)
Rated speed, $n$	>1400 rpm
Number of poles, $2p$	4
Rated frequency, $f$	50 Hz
Synch. speed, $n_s$	1500 rpm
Efficiency, $\eta$	$\geq 0.8$
Power factor, $\cos \varphi$	$\geq 0.9$
Rated voltage, $U_N$	230 V
Rated current, $I_N$	$\leq 5$ A
Starting current ratio, $I_{st}/I_N$	$\leq 4.5$
Rated torque, $T_N$	$\geq 5$ Nm
Starting torque ratio, $T_{st}/T_N$	$\leq 0.35$
Net mass, $M$	<14.0 kg
Mounting	foot
Insulation class	B
Design type	N

**TABLE A2** Values of single-phase induction motor design parameters

Parameter	Symbol	Value used	Typical industrial values
Average airgap flux density	$B_g$ , T	0.80	0.50-0.90
Stator core magnetic flux density	$B_{cs}$ , T	1.40	1.30-1.70
Stator magnetic flux density at teeth	$B_{ts}$ , T	1.35	0.80-1.00 $B_{cs}$
Stator slot opening width	$b_{s0}$ , mm	2.50	2.00-3.00
Stator slot height at teeth	$h_{s0}$ , mm	0.80	0.50-1.00
Stator teeth side height	$h_{s1}$ , mm	1.00	1.00-4.00
Rotor core magnetic flux density	$B_{cr}$ , T	1.40	1.40-1.70
Rotor magnetic flux density at teeth	$B_{tr}$ , T	1.35	0.80-1.00 $B_{cr}$
Rotor slot opening width	$b_{r0}$ , mm	1.00	2.00-3.00
Rotor slot height at teeth	$h_{r0}$ , mm	1.00	0.50-1.00
Rotor teeth side height	$h_{r1}$ , mm	1.00	0.80-1.50
Saturation factor	$k_{sat}$	0.90	0.70-0.90
Winding factor for main winding	$k_{wm}$	0.80	0.75-0.85
Rotor to stator slot area ratio	$k_A$	0.38	0.35-0.60
Transformation ratio	$\alpha$	1.50	1.00-2.00

**TABLE A3** Performance and geometrical characteristics comparison of sample single-phase induction motor design

	Classical Design	Proposed Approach	Variation, %
Outer stator diameter, $D_o$ , mm	158.76	137.87	− 13.15
Inner stator diameter, $D$ , mm	95.25	83.41	− 12.43
Outer rotor diameter, $D_r$ , mm	94.58	82.82	− 12.43
Shaft diameter, $D_{sh}$ , mm	40.15	36.09	− 10.11
Active axial core length, $L$ , mm	94.25	125	+ 32.62
Airgap length, $g$ , mm	0.338	0.295	− 12.72
Volume, $V$ , cm <sup>3</sup>	1864.80	1865.17	+ 0.02
Net mass, $M$ , kg	13.88	13.147	− 5.27
Efficiency, $\eta$	85.06	85.702	+ 0.74
Power factor, $\cos \varphi$	0.98	0.9912	+ 0.30
Phase shift, $\theta$ , deg	74.70	75.42	+ 0.97
Rated current, $I_N$ , A	3.91	3.84	− 1.78
Starting current, $I_{st}$ , A	15.85	16.25	+ 2.53
Starting to rated current ratio $I_{st}/I_N$	4.05	4.23	+ 4.38
Rated torque, $T_N$ , Nm	4.87	5.00	+ 2.72
Starting torque, $T_{st}$ , Nm	0.10	0.15	+ 55.80
Starting to rated torque ratio $T_{st}/T_N$	0.02	0.03	+ 51.66
Power density, $P_d$ , W/kg	54.03	57.04	+ 5.56

**TABLE A4** Main and auxiliary windings characteristics of the qualifying single-phase induction motor models (see Tables 2-4 )

	$Q_s$	$Q_r$	$R_m$	$X_m$	$R_a$	$X_a$	$N_m$	$N_a$	$N_a/N_m$
Copper	36	18	4.16	3.11	6.58	5.43	428	512	1.196
	36	14	4.16	3.11	6.66	5.57	428	520	1.214
	24	14	4.09	4.38	5.76	7.63	416	496	1.192
	24	10	4.09	4.41	6.76	8.42	416	520	1.250
	12	36	5.05	16.54	5.34	20.42	456	460	1.008
Aluminum	36	22	4.16	3.11	6.52	5.32	428	508	1.186
	36	20	4.16	3.11	6.58	5.43	428	512	1.196
	24	14	4.09	4.38	6.55	7.86	416	504	1.211
	24	10	4.09	4.42	6.82	8.57	416	524	1.259
	12	36	5.05	16.62	5.39	20.88	456	464	1.017
Magnesium	36	26	4.16	3.11	6.58	5.42	428	512	1.196
	36	22	4.16	3.11	6.61	5.47	428	516	1.205
	24	34	4.09	4.32	5.72	7.42	416	492	1.182
	24	14	4.09	4.38	6.55	7.86	416	504	1.211
	12	36	5.05	16.65	5.44	21.28	456	468	1.026